Saturated Absorption Spectroscopy: Elimination of Crossover Resonances with the Use of a Nanocell

A. Sargsyan[a], D. Sarkisyan[a], A. Papoyan[a,] *, Y. Pashayan-Leroy[b], P. Moroshkin[c], A. Weis[c], A. Khanbekyan[d], E. Mariotti[d], and L. Moi[d]

[a] *Institute for Physical Research, National Academy of Sciences of Armenia, Ashtarak, 0203 Armenia*
[b] *Institut Carnot de Bourgogne, UMR 5209 CNRS-Université de Bourgogne, F-21078 Dijon Cedex, France*
[c] *Département de Physique, Universite de Fribourg, Chemin du Musee 3, 1700 Fribourg, Switzerland*
[d] *CNISM-Department of Physics, University of Siena, Via Roma 56, 53100 Siena, Italy*
*e-mail: papoyan@ipr.sci.am

Abstract—It is demonstrated that the velocity-selective optical pumping/saturation resonances of the reduced absorption in a Rb vapor nanocell with thickness $L = \lambda$, 2λ, and 3λ (resonant wavelength $\lambda = 780$ nm) allow for the complete elimination of crossover (CO) resonances. We observe well-pronounced resonances corresponding to the $F_g = 3 \longrightarrow F_e = 2$, 3, and 4 hyperfine transitions of the ^{85}Rb D_2 line with line widths close to the natural width. A small CO resonance located midway between $F_g = 3 \longrightarrow F_e = 3$ and $F_g = 3 \longrightarrow F_e = 4$ transitions appears only for $L \geq 4\lambda$. The D_2 line ($\lambda = 852$ nm) in a Cs nanocell exhibits a similar behavior. From the amplitude ratio of the CO and VSOP resonances, it is possible to determine the thickness of the column of alkali vapor in the range of 1–1000 μm. The absence of the CO resonances for nanocells with $L \sim \lambda$ is attractive for the frequency reference application and for studying the transitions between the Zeeman sublevels in external magnetic fields.

PACS numbers: 32.70.Jz, 42.62.Fi, 32.10.Fn, 42.50.Hz

INTRODUCTION

Saturated absorption (SA) spectroscopy is widely used in the realization of frequency references for atomic transitions [1–3]. In this technique, the laser beam is split into a weak probe field and a strong pump field, which are sent to the interaction cell as counterpropagating overlapping beams. Because of opposite Doppler shifts, only the atoms moving perpendicular to the radiation propagation direction resonantly interact with both laser beams. For these atoms, the pump beam saturates the transition, and the absorption spectrum of the probe shows a Doppler-free dip, the so-called velocity selective optical pumping/saturation (VSOP) resonance located at the line center. With properly chosen pump and probe beam intensities, careful adjustment of the geometry, and the elimination of stray magnetic fields, the line width of the resonance (to which we refer to as "VSOP resonance") may be as narrow as the natural width of the transition.

The situation is more complex when two or more atomic (hyperfine) transitions overlap within the Doppler profile, which is the case for the majority of real atomic lines. The presence of multiple unresolved hyperfine transitions results in the formation of the so-called crossover (CO) resonances. These "spurious" resonances appear when the laser frequency is tuned midway between two transitions, so that, for a group of atoms moving with a certain longitudinal velocity, the pump beam drives one transition, while the probe drives the other one linked to the former by the same ground state. As a result of the partial depletion of the ground state by the pump beam, the probe "sees" a reduced absorption. Thus, the VSOP process is also responsible for the occurrence of CO resonances. The CO resonances may seriously complicate the applicability of the SA spectral reference technique, notably in the high-resolution spectroscopy of hyperfine levels with a small (10–30 MHz) frequency spacing. In that case, the CO resonances mask the real atomic VSOP resonances and, thus, hinder or even impede the identification of the relevant spectral features. We note that, as a rule, the amplitude of the CO resonances is larger than the one for the actual VSOP resonances.

There are several techniques that allow for the elimination of crossover resonances in atomic vapors. In [4], two *copropagating* laser beams (a pump laser with a fixed frequency and a probe laser with a tunable frequency) were used rather than *two counterpropagating* beams. In [5], it was shown that the use of a thin (20 μm-long) cell in a conventional SA setup allows for the reduction of the amplitude of the CO resonance. Note that the optical selective reflection (SR) spectroscopy technique [6, 7] also allows one to eliminate the CO resonances; but, for the correct determination of an atomic transition position using this technique, the spectra must undergo further nontrivial processing.

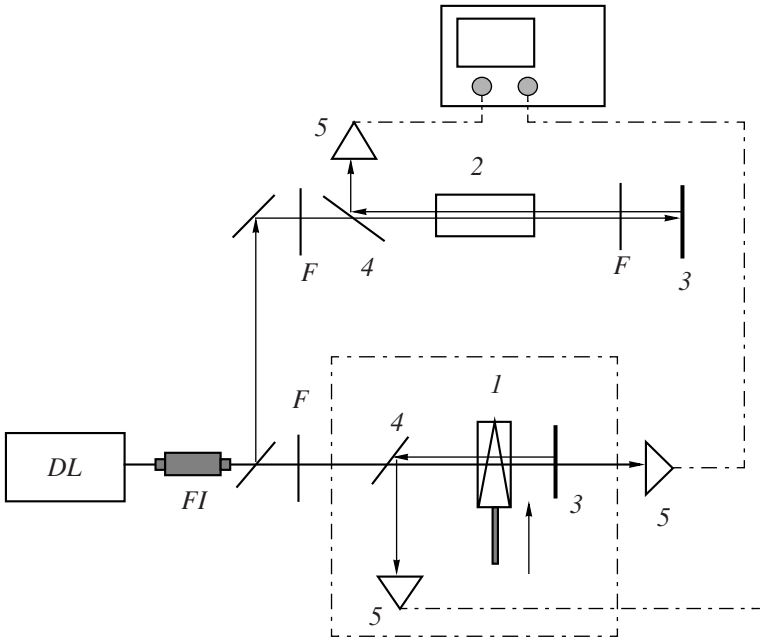

Fig. 1. Experimental setup. *DL*—tunable diode laser, λ = 780 nm (852 nm); *FI*—Faraday isolator; *1*—Rb (Cs) cell with nanometric, micrometric, or an ordinary thickness (see the text); *F*—neutral density filters; *2*—Rb (Cs) cell of an ordinary length; *3*—mirror; *4*—glass plate; *5*—photodiodes.

In this work, we aim at revealing the minimal thickness L of the atomic vapor layer needed for the formation of the CO resonance, and studies of the further evolution of the CO development as L increases. We also examine and demonstrate the advantages of using very small (wavelength-scale) thicknesses L of the atomic vapor column (a "nanocell") as a promising spectroscopic tool. We show that, by using nanocells, it is possible to completely eliminate the CO resonances. This advantage (along with several others) makes the use of a nanocell with the thickness $L = \lambda$, 2λ, and 3λ as a frequency reference for an atomic transition attractive. It is shown that the absence of CO is of significant importance, particularly for the study of the Zeeman spectra of the ^{87}Rb D_2 line in an external magnetic field.

EXPERIMENTAL SETUP

The scheme of the experimental setup is presented in Fig. 1. The beam from a single-frequency tunable diode laser (1-mm diameter, power $P_L = 30$ mW, central wavelength λ = 780 nm, and line width $\gamma_L \sim 5$ MHz) irradiated thin cell *1* under an incidence angle close to the normal. A Faraday isolator (*FI*) was inserted to prevent the optical feedback to the laser. In the experiment, we used different cells *1* with various thicknesses L in the ranges $L = \lambda$–6λ (nanometric, vertical wedged-shaped vapor column) [8–11]; 9, 60, and 700 μm and 2-, 4-, and 60-mm-long. The cell was inserted into an oven with two apertures for passing the radiation. The Rb density determining the temperature of the cell's side arm was adjusted in the range of 40–115°C, depending on the cell thickness. To prevent the atomic vapor condensation on the cell windows, their temperature was kept 20° to 30° higher that the side-arm temperature. The laser intensity was controlled by neutral density filters F and its frequency scanned over ~10 GHz, covering the hyperfine spectral components of the ^{85}Rb D_2 lines $F_g = 3 \longrightarrow F_e = 2$, 3, and 4, where the subscripts g and e refer to the lower and upper levels, respectively. Mirror *3* and glass plate *4* (shown in Fig. 1 inside the dotted rectangle) were used to form the SA spectra. In order to vary thicknesses L of the vapor column in the nanocell in the range $L = (1$–$6)\lambda$, the oven was translated along the vertical direction as indicated by the arrow in Fig. 1. A part of the laser beam was sent to a normal vapor cell with a thickness of 60 mm to obtain a reference SA spectrum. The upper set of filters *F* was used to properly attenuate the laser beam in order to get the reference SA spectra with a line width close to the natural width. The spectra were registered by a four-channel digital storage oscilloscope (Tektronix, TDS 2014B).

RESULTS AND DISCUSSION

It was shown earlier [9–12] that the ratio L/λ, where L is the thickness of the atomic vapor column and λ is the laser wavelength resonant with the atomic transition, is an important parameter that determines the widths, shapes, and amplitudes of the absorption resonances in a nanocell. In particular, it was shown that the spectral width of the resonant absorption is minimal for $L = (2n + 1)\lambda/2$ (where n is an integer), an effect which

was called the "Dicke-type coherent narrowing effect" (DCNE). It was also shown that, for $L = n\lambda$, the spectral width of the resonant absorption reaches a maximal value close to the Doppler width (about several hundreds of MHz), an effect called collapse of DCNE [9, 10]. In [13], the DCNE and the collapse of DCNE were investigated up to thicknesses $L = 6\lambda$ for the D_1 line of Cs at $\lambda = 894$ nm. Here, we consider the case where $L = n\lambda$, since as was shown in [10, 11], the VSOP resonances appear under this condition.

In Fig. 2, the transmission spectra are presented for L varying in the range from $L = \lambda$ up to 6λ with steps of λ (for these recordings, mirror *3* and glass plate *4* were removed). The effective laser intensity (EI) is determined by multiplying the measured intensity by the coefficient $[\gamma_N/(\gamma_N + \gamma_L)]$, where γ_N is the spontaneous decay rate of the Rb D_2 line, $\gamma_L \sim 5$ MHz, and EI is 10 mW/cm^2. When L is varied from $L = \lambda$ to 3λ, it can be seen that only the VSOP resonances are detected. These peaks of a decreased absorption are located exactly at the atomic transition frequencies [5, 10–13], and arise because the atom in the ground level $F_g = 3$ absorbs a laser photon populating the excited level followed by the spontaneous decay to the ground level $F_g = 2$ or 3, an effect well known as optical pumping (OP) [1–3, 5, 12] (peculiarities of the OP process in a submillimeter-thin cell are presented in [14, 15]). As a result, a fraction of the atoms populates the $F_g = 2$ level, and the number of atoms absorbing from the $F_g = 3$ level is reduced. As a consequence, the absorption from this level decreases. The efficiency of OP is determined by the expression

$$\eta \sim \frac{\Omega^2 \gamma_N t}{(\Delta + \mathbf{kv})^2 + \Gamma^2}, \qquad (1)$$

where t is the average interaction time of the atom with the radiation field, v is the atomic velocity, Δ is the detuning, Γ is the sum of homogeneous and inhomogeneous broadenings, and $k = 2\pi/\lambda$ [12]. Equation (1) shows how the optical pumping efficiency grows with the interaction time t. For atoms flying perpendicularly to the laser beam, the interaction time is $t_D = D/v$, where D is the laser beam diameter, while atoms flying along the laser beam have an interaction time of $t_L = L/v$. Since $D \sim 1$ mm and $L = 780$ nm (or 852 nm in the case of Cs), t_D exceeds t_L by three orders of magnitude. For atoms flying perpendicular to the laser beam, $\mathbf{k} \cdot \mathbf{v} = 0$ and the efficiency in Eq. (1) becomes maximal for $\Delta = 0$. For this reason, the VSOP peak is centered exactly at the atomic transition frequency [5, 10–12]. Note that there is a reflected beam from the inner surface of the nanocell, which propagates backwards with respect to the main beam, and this beam may cause the formation of the CO resonance. However, the interaction time t_L for atoms with a longitudinal velocity, $v_z = 2\pi\varepsilon/k$ (where ε is half of the frequency separation of the corresponding excited levels) along the laser beam is rather small for $L = \lambda$, 2λ, and 3λ to provide efficient optical pumping, which is needed for the CO resonance formation (in our case, 2ε is 121 and 63 MHz, respectively).

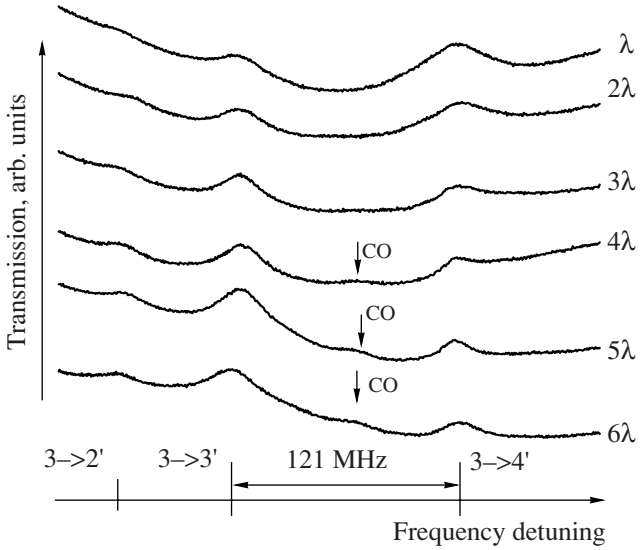

Fig. 2. Transmission spectra of the nanocell for the transitions $F_g = 3 \longrightarrow F_e = 2$, 3, and 4 of the ^{85}Rb D_2 line, for L varying in the range λ–6λ. The effective laser intensity was ~10 mW/cm^2. The temperature of the cell's side arm is 115°C. The CO resonances are marked by arrows.

However, as can be seen from Fig. 2, a small CO resonance (marked by arrows) located midway between the $F_g = 3 \longrightarrow F_e = 3$ and $F_g = 3 \longrightarrow F_e = 4$ transitions appears in the transmission spectra when the thickness $L \geq 4\lambda$. One can also see a different behavior for the VSOP peaks at different transitions. It is interesting to note that, when $L = \lambda$, the amplitude ratios of the VSOP peaks is close to the ratio of the atomic probabilities of the corresponding transitions $F_g = 3 \longrightarrow F_e = 2$, 3, and 4, i.e., $A(3–4')/A(3–3') \sim 2$, $A(3–3')/A(3–2') \sim 3$ [16], while for the SA spectrum, this is not the case (compare with the lower curve of Fig. 4). As the thickness increases, the amplitude of the VSOP peak corresponding to the $F_g = 3 \longrightarrow F_e = 4$ cycling transition decreases, while the amplitudes of the VSOP peaks for the noncycling transitions $F_g = 3 \longrightarrow F_e = 2$, 3 increase. In particular, for $L = 6\lambda$ the ratio $A(3–4')/A(3–3') \sim 0.5$. Conversely, the ratio of the noncycling transitions is practically independent of the thickness, i.e., $A(3–3')/A(3–2') \sim 3$. Figure 3 presents the theoretical spectra for the same group of transitions calculated using the model presented in [13]. All of the important experimental parameters determining the VSOP resonance formation, such as the influence of the reflected beam by the second wall of the nanocell (which is important when the thickness $L \sim \lambda$), the line width and intensity of the laser, the type of atomic transition (cycling or noncycling), the Maxwellian velocity distribution of the atoms, etc. have been taken into account. The fol-

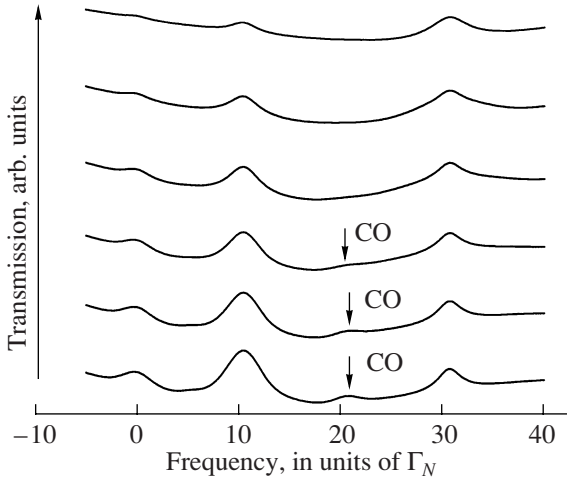

Fig. 3. Calculated spectra for the conditions in Fig. 2. Rabi frequency $\Omega = 0.4\gamma_N$; $\gamma_L = 5$ MHz; and $\gamma_N = 6$ MHz.

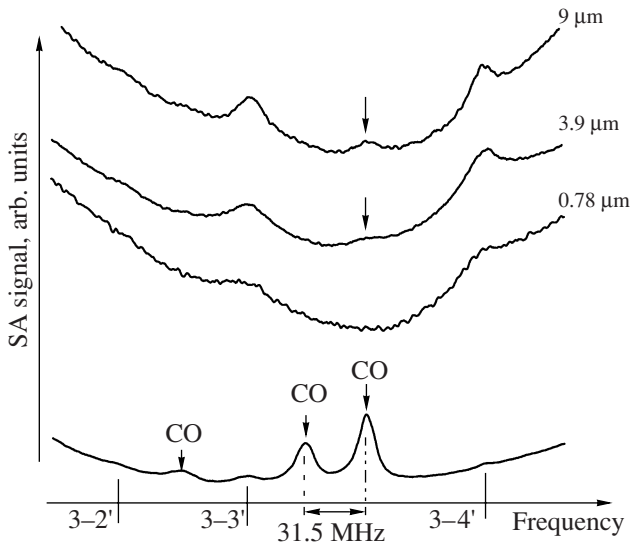

Fig. 4. Saturated absorption spectra for Rb cells with L = 780 nm, 3.9 μm, and 9.0 μm. The lower curve is the SA spectrum of an ordinary 60-mm-long cell. The CO resonances are marked by the arrows.

lowing parameters were used in the calculations: natural line width $\gamma_N = 6$ MHz, Rabi frequency $\Omega = 0.4\gamma_N$, and laser line width $\gamma_L = 5$ MHz. One sees that the theoretical model [13] correctly describes the peculiarities of the VSOP of the cycling and noncycling transitions as well as the behavior of the CO resonance as a function of the thickness L. One can conclude from Figs. 2 and 3 that the optimum condition for the formation of an atomic reference spectrum (e.g., to determine the frequency position of a weak atomic transition as $F_g = 3 \longrightarrow F_e = 2$) is obtained for $L = 3\lambda$, in which case, the narrow and large VSOP peaks are observed, along with the absence of the CO resonances.

The second set of measurements was done for the same group of transitions employing the SA configuration (mirror *3* and glass plate *4* are mounted as shown in Fig. 1). Thin cells with thicknesses $L = \lambda$ (780 nm), 5λ (3.9 μm), 9, 60, and 700 μm and cells with a length of 2, 4, and 60 mm have been used.

In Fig. 4, the SA spectra are presented for $L = \lambda$ (780 nm), 5λ (3.9 μm), and 9 μm. The lower curve is the SA spectrum recorded in a 60-mm-long cell serving as the reference. As before, the CO resonance is completely absent in the case of $L = \lambda$, while it appears when $L = 5\lambda$ (3.9 μm) and the amplitude of the CO resonance increases as L increases from 3.9 to 9.0 μm.

Figure 5 shows the SA spectra for $L = 60$ μm, 0.7, 2, and 4 mm. The VSOP resonance of the $F_g = 3 \longrightarrow F_e = 4$ transition is sensitive to the polarizations of the pump and probe beams [17]. For a quantitative description, it is, therefore, more convenient to use the ratio of the amplitude of the CO resonance appearing when the laser is tuned midway between the $F_g = 3 \longrightarrow F_e = 3$ and $F_g = 3 \longrightarrow F_e = 4$ atomic transitions (this is the largest CO resonance in the spectrum), and the amplitude of the VSOP resonance of the $F_g = 3 \longrightarrow F_e = 3$ transition. Figure 6 shows the ratio of A(CO)/A(VSOP 3–3') as a function of the cell thickness. The monotonic smooth increase of this dependence permits us to infer the cell thickness from a measurement of the amplitude ratio. Note that, in the case of thinner cells ($L \sim \lambda$), the interferometric method presented in [9] allows for the determination of the thickness L with a high accuracy (~15 nm). It should be noted that the dependence shown in Fig. 6 is slightly affected by the pump and probe beam intensities, and is correct for the ^{85}Rb, $F_g = 3 \longrightarrow F_e = 2$, 3, and 4 atomic transitions.

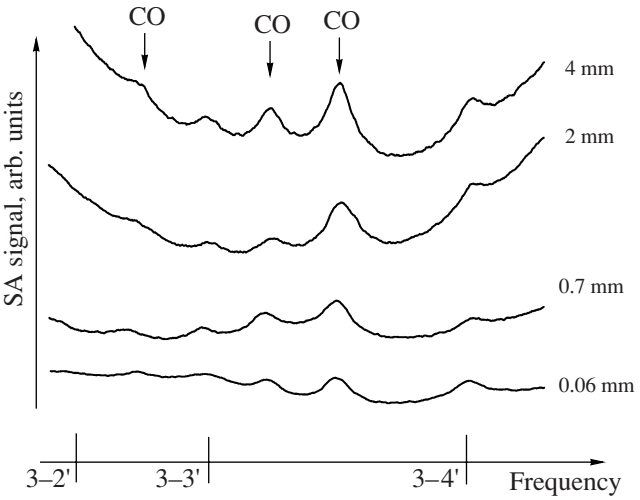

Fig. 5. Saturated absorption spectra for Rb cells with L = 60 μm, 0.7, 2.0, and 4.0 mm.

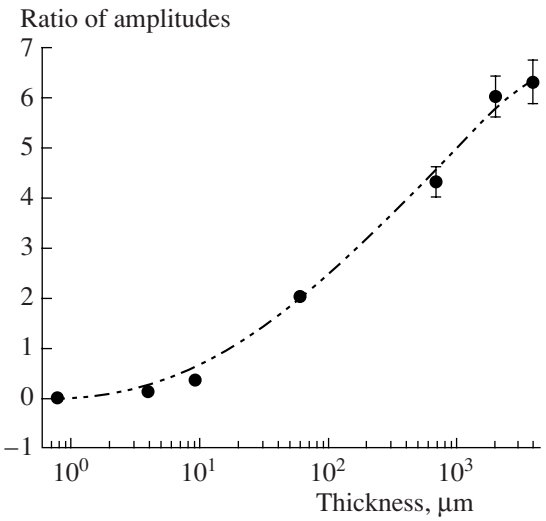

Fig. 6. Amplitude ratios A(CO)/A(VSOP 3–3') as a function of the cell thickness. The dotted line is shown to guide the eye.

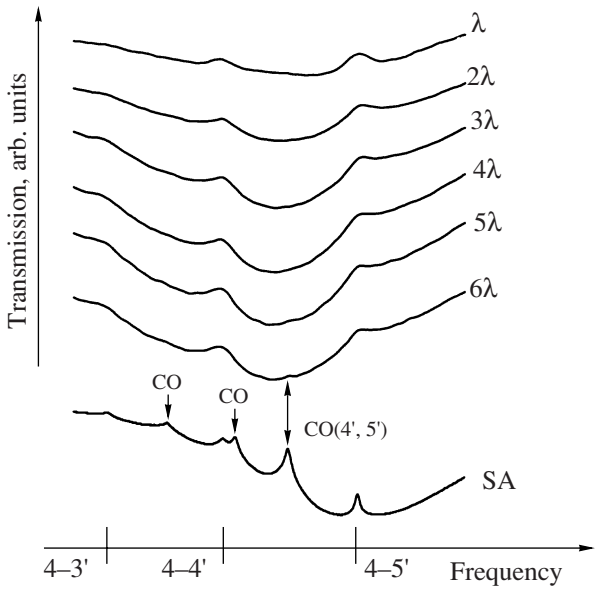

Fig. 7. Transmission spectra of the Cs nanocell for the transitions $F_g = 4 \longrightarrow F_e = 3$, 4, and 5 for the ^{133}Cs D_2 line, for L varying in the range λ–6λ. The effective laser intensity is ~10 mW/cm^2. The temperature of the side arm is 110°C. The lower curve is the SA spectrum in an ordinary cell. The CO resonances are marked by the arrows.

There are several parameters which influence the CO resonance amplitude, in particular, the frequency separation between the upper levels (2ε), the probabilities of the atomic transitions involved in the CO resonance formation, and the thermal atomic velocity of the alkali atom [2, 3]. A frequency-tunable distributed feedback diode laser with λ = 852 nm (line width 5 MHz) and EI ~10 mW/cm^2 has been used to obtain the transmission spectra (see Fig. 7) for a nanocell filled with a Cs vapor for L varying in the range of λ to 6λ in steps of λ ($F_g = 4 \longrightarrow F_e = 3$, 4, and 5 transitions of the D_2 line). In this case, a small CO resonance appears at $L = 6\lambda$ when the laser is tuned midway between the $F_g = 4 \longrightarrow F_e = 4$ and $F_g = 4 \longrightarrow F_e = 5$ atomic transitions. This is in agreement with the results presented in [5], where the ratio A(CO)/A(VSOP 4–4') is ≈0.4 for the $F_g = 4 \longrightarrow F_e = 3$, 4, and 5 transitions in Cs and L = 100 μm, while for the $F_g = 3 \longrightarrow F_e = 2$, 3, and 4 group in ^{85}Rb, the ratio A(CO)/A(VSOP 3–3') is ≈2 at an even smaller cell thickness (L = 60 μm) (see Fig. 5). Note that, when $L = \lambda$, the amplitude ratio of the VSOP peaks is close to the ratio of the atomic probabilities of the corresponding transitions (as can be seen in Fig. 2 for the Rb), while, for the SA spectrum, it is again not the case (compare to the lower curve of Fig. 7).

The difference between the SA spectra for different atomic transitions is well seen if we compare spectra obtained in similar conditions (i.e., cell length, temperature, laser intensity, etc.), as is the case for the lower traces of Figs. 4 and 7 (^{85}Rb D_2 line, $F_g = 3 \longrightarrow F_e = 2$, 3, and 4 in Fig. 4, and the Cs D_2 line, $F_g = 4 \longrightarrow F_e =$ 3, 4, and 5 in Fig. 7). For ^{85}Rb, the ratio A(CO)/A(VSOP 3–3') is ~ 10, while for Cs, we find A(CO)/A(VSOP 4–4') ~ 2. Similar ratios can be also seen in [2, 3]. From this behavior, one can expect that for the case of the Cs $F_g = 4 \longrightarrow F_e = 3$, 4, and 5 transitions, the increase of the CO resonance amplitude with that thickness should be somewhat weaker.

It is well known that atoms placed in an external magnetic field undergo shifts of their energy levels and changes in their transition probabilities [18]. In [19], in order to realize these studies for the ^{87}Rb D_2 line with the elimination of the Doppler broadening, the SA technique has been used. In particular, the atomic transitions $F_g = 1 \longrightarrow F_e = 0$, 1, and 2 have been studied. The complexity of the Zeeman spectra in the magnetic field arises primarily from the presence of strong crossover resonances, which are also split into many components. Hence, in [19], it was possible to study only the behavior of the total value of the sum of the VSOP and CO amplitudes inside the Zeeman spectra.

The use of the nanocell allows one to study the shift of the energy levels and the change in the transition probability for an individual atomic transition. In Fig. 8a, the middle curve is the transmission spectrum from the reference nanocell, which shows the positions of the $F_g = 1 \longrightarrow F_e = 0$, 1, and 2 atomic transitions, i.e., of the VSOP resonances for $B = 0$. In the upper curve, the transmission spectrum is given from the nanocell for $B \approx 30$ G (directed along the laser beam) with σ^+-polarized excitation (numbers denote transitions marked in Fig. 8b). The splitting and shifts of the three VSOP resonances *6*, *5*, and *4* are seen clearly in Fig. 8a. For $B = 0$, the theoretical ratio of these transition probabilities is 6 : 3 : 1 (corresponding to the VSOP reso-

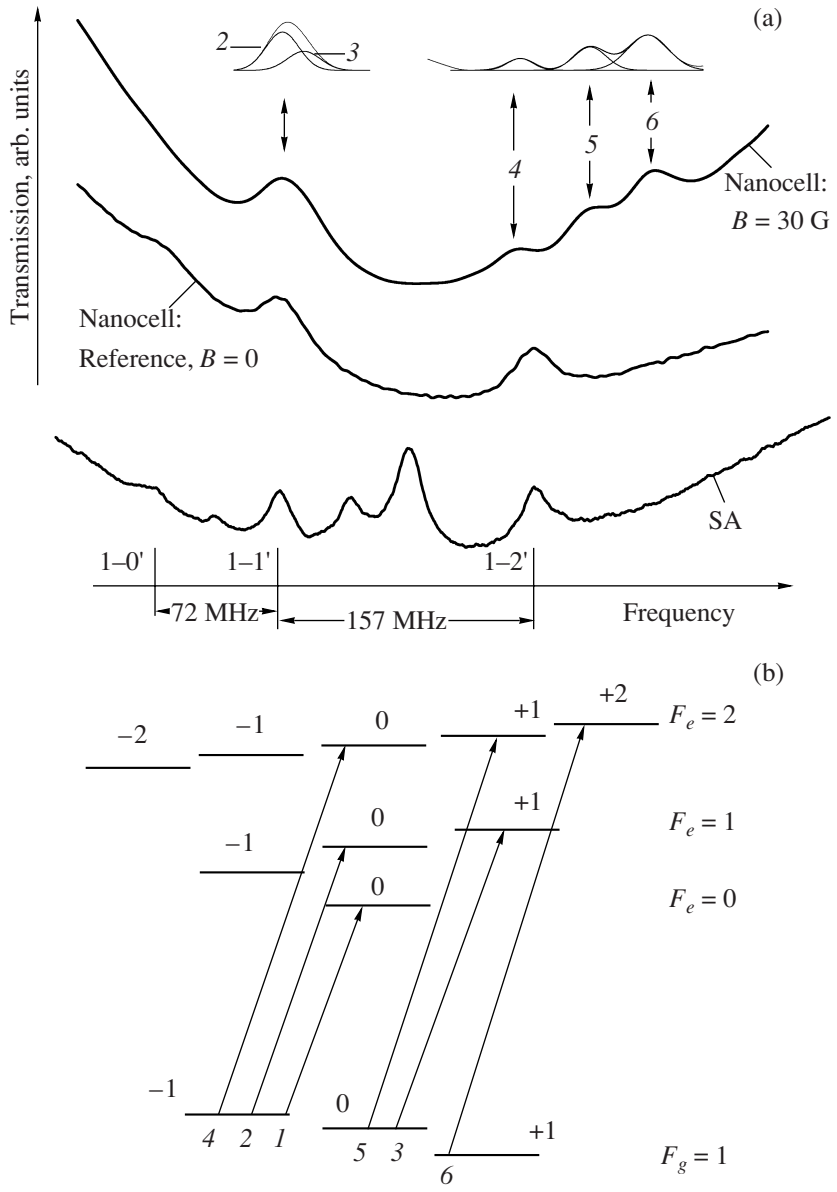

Fig. 8. (a) The upper curve is the transmission spectrum of a σ^+-polarized laser on $F_g = 1 \longrightarrow F_e = 0$, 1, and 2 hyperfine transitions of the ^{87}Rb D_2 line in the nanocell for $B \approx 30$ G. The middle curve is the transmission spectrum from the reference nanocell for $B = 0$. The lower curve is the SA spectrum for $B = 0$. (b) Partial energy level diagram of the D_2 line of ^{87}Rb in a magnetic field and possible atomic transitions for σ^+-polarized exciting laser radiation.

nances numbered *6*, *5*, and *4*), while for $B = 30$ G, the ratio of probabilities (corresponding actually to the amplitudes of VSOP resonances) is 6 : 4 : 3. As to the VSOP peaks *2* and *3*, they are spectrally partially overlapped, as shown in the left inset. The theoretical ratio of the probabilities for $B = 0$ is equal to 1, while for $B = 30$ G, the ratio is equal to 2. The transition $F_g = 1$, $m_F = -1 \longrightarrow F_e = 0$, and $m_F = 0$ (numbered *1*) is almost invisible in Fig. 8a, because its probability (i.e., VSOP amplitude) for $B \approx 30$ G practically vanishes. The calculated probabilities are presented in [20], and a good agreement is observed between experiment and theory. The SA spectrum is presented in Fig. 8a by the lower curve for $B = 0$ (for the SA in a magnetic field, see [19, Fig. 6]).

Note that Fig. 8a (the upper curve) enables one to determine the frequency shift of the atomic transitions from their initial positions in a zero magnetic field (the middle curve) and, thus, allows one to determine the external magnetic field with a submicron (780 nm) spatial resolution. This is important for the mapping of a strongly inhomogeneous magnetic field.

Since, for Na atoms, the resonant wavelength of the D line is the smallest (≈590 nm) as compared with that

of other alkali metals, one can expect the best spatial resolution when using a Na nanocell. For this purpose, we have recently prepared a nanocell filled with Na metal. The thickness L of the gap between the windows has a wedge in the vertical direction varying from 100 to 550 nm at room temperature. At the windows' operating temperature of ~200°C, the maximum thickness L slightly increases, reaching 800 nm. Thus, there is a region of thickness $L = \lambda$ where the Zeeman spectra can be obtained. This experiment is in progress at the University of Siena.

CONCLUSIONS

We have demonstrated that the use of a nanocell as the frequency reference for atomic transitions in comparison with the use of the SA spectra provides several advantages as follows: (i) contrary to SA, in the case of a nanocell, the crossover lines are absent, and this is very important for the study of the Zeeman spectra; (ii) for the case of a nanocell with thickness $L = \lambda$, the ratio of the amplitudes for the VSOP peaks is close to the ratio of the atomic probabilities of the corresponding transitions, while in the case of SA, this is not the case; moreover, as a rule, a strong cycling transition in the SA spectrum has a smaller amplitude in comparison with that of the weaker noncycling one; (iii) the SA geometry requires counterpropagating beams, while a single-beam transmission spectrum is needed for a nanocell; and (iv) the laser power needed for spectral reference applications in the case of a nanocell is more than an order of magnitude less than that needed for SA.

From the ratio of the amplitudes of the CO and VSOP resonances, it is possible to determine the thickness of the alkali vapor column in the range from 1 to 1000 μm.

It is important to note that the absence of CO resonances in a nanocell with $L \sim \lambda$ allows one to study the behavior of the atomic transitions between the Zeeman sublevels in an external magnetic field, since the short time of flight ensures that the CO resonances are absent, even when the VSOP resonance is split into several Zeeman components. Conversely, even if the CO resonances are absent in the SA spectrum of an ordinary cell (this happens when the frequency distance between the upper levels is larger than the Doppler width of the atomic transition), the CO resonance may appear again (due to the large time of flight) when the VSOP resonance is split into several components.

ACKNOWLEDGMENTS

D.S. is grateful to the University of Siena for its hospitality. A.S, D.S, A.P, Y.P-L, E.M., and L.M. are thankful for the financial support provided by INTAS South-Caucasus (grant no. 06-1000017-9001). A.S, D.S, A.P, P.M., and A.W. are thankful for financial support provided by SCOPES (grant no. IB7320-110684/1).

REFERENCES

1. W. Demtröder, *Laser Spectroscopy* (Springer-Verlag, Berlin, 1982; Nauka, Moscow, 1985).
2. O. Schmidt, K.-M. Knaak, R. Wynands, and D. Meschede, Appl. Phys. B **59**, 167 (1994).
3. D. A. Smith and I. G. Hughes, Am. J. Phys. **72**, 631 (2004).
4. A. Banerjee and V. Natarajan, Opt. Lett. **28**, 1912 (2003).
5. S. Briaudeau, D. Bloch, and M. Ducloy, Phys. Rev. A *59*, 3723 (1999).
6. R. Müller and A. Weis, Appl. Phys. B **66**, 323 (1998).
7. H. Failache, S. Saltiel, M. Fichet, et al., Phys. Rev. Lett. **83**, 5467 (1999).
8. D. Sarkisyan, D. Bloch, A. Papoyan, and M. Ducloy, Opt. Commun. **200**, 201 (2001).
9. G. Dutier, A. Yarovitski, et al., Europhys. Lett. **63** (3), 35 (2003).
10. D. Sarkisyan, T. Varzhapetyan, et al., Phys. Rev. A **69**, 065802 (2004).
11. C. Andreeva, S. Cartaleva, et al., Phys. Rev. A **76**, 013837 (2007).
12. G. Nikogosyan, D. Sarkisyan, and Yu. Malakyan, J. Opt. Technol. **71**, 602 (2004).
13. A. Sargsyan, D. Sarkisyan, Y. Pashayan-Leroy, et al., http://eprintweb.org/s/archive/physics/0707.0379.
14. A. Ch. Izmailov, K. Fukuda, M. Kinoshita, and M. Tachikawa, Laser Phys. **14** (1), 30 (2004).
15. A. Ch. Izmailov, Laser Phys. Lett. **3** (1), 132 (2006).
16. D. Sarkisyan, T. Becker, A. Papoyan, et al., Appl. Phys. B **76**, 625 (2003).
17. C. P. Pearman, C. S. Adams, et al., J. Phys. B: At. Mol. Opt. Phys. **35**, 5141 (2002).
18. P. Tremblay, A. Michaud, M. Levesque, et al., Phys. Rev. A **42**, 2766 (1990).
19. M. Ummal Momeen, G. Rangarajan, P. C. Deshmukh, J. Phys. B: At. Mol. Opt. Phys. **40**, 3163 (2007).
20. T. Varzhapetyan, H. Hakhumyan, D. Sarkisyan, et al., J. Contemp. Phys. **42**, 223 (2007).